Nb-doping Induced High Coercivity in $Pr_2Fe_{14}B$/α-Fe Nanocomposite Melt-spun Ribbons

Shuang FU [1], Mehran Khan ALAM [2, 3], Guangbing HAN[3] *, Shishou KANG [3]

[1] *School of Medical Information Engineering, Shandong University of Traditional Chinese Medicine, 250355, Jinan, China*
[2] *School of Material Science and Engineering, Shandong University, 250061, Jinan, China*
[3] *School of Physics, Shandong University, 250100, Jinan, China*

http://doi.org/10.5755/j02.ms.43624

Received 18 November 2025; accepted 20 February 2026

The effect of niobium (Nb) doping on the microstructure and magnetic properties of as-spun $Pr_{10}Fe_{82.5-x}B_{6.5}Nb_x$ ribbons was investigated. Nb doping significantly refines the grain size and enhances the coercivity, which increases from 380 kA/m (x = 0) to a remarkable 990 kA/m (x = 3), a top-level performance among Nb-doped rare-earth-deficient nanocomposite alloys. The improvement is attributed to the microstructural refinement and a shift in the magnetization reversal mechanism toward dominant domain-wall pinning. Recoil loop measurements further confirm that Nb doping strengthens the intergranular exchange coupling. This work demonstrates that Nb doping is a feasible and efficient approach for producing cost-effective, high-performance permanent magnets with low rare-earth content.
Keywords: coercivity, nanocomposite ribbons, niobium doping, melt spinning, low rare-earth content.

1. INTRODUCTION

Although sintered $Nd_2Fe_{14}B$ magnets have excellent performance, their production and application costs have always been high due to the complexity of raw material supply and production processes, as well as poor chemical stability and susceptibility to corrosion [1]. Nanocomposite permanent magnets, with less rare earth content, have garnered significant interest owing to their enhanced properties, such as greater thermal stability, better resistance to corrosion, and lower production costs [2], which have broad applications in fields such as advanced materials, machinery, environmental engineering, healthcare, and biomedical science. Although these magnets have a theoretical maximum energy product ($(BH)_{max}$) of approximately 1000 kJ/m^3, this value is considerably higher than that typically achieved in practice [3 – 5]. This gap is largely attributed to the difficulty in attaining an optimal microstructure [6]. Hence, microstructural refinement is crucial for enhancing the magnetic properties.

In 1984, Croat et al. developed an Nd-Fe-B alloy using the melt-spinning technique, a process that is still extensively adopted for the preparation of such nanocomposite magnets [7], because it is easy to control the grain size by changing the wheel speed. Additionally, element doping and heat treatment can refine the microstructure and have a significant effect on the magnetic properties [8]. Niobium (Nb) is widely regarded as one of the most effective elements for enhancing the magnetic properties of melt-spun ribbons. The addition of Nb to $Nd_{11}Dy_{0.5}Fe_{80.4}Nb_2B_{6.1}$ refines the grain size and texture, resulting in enhanced coercivity from 150 kA/m (0 at % Nb) to 563 kA/m (2 at % Nb) in the hot-deformed state [9]. Similarly, the addition of 1 at % Nb to $(Nd_{0.9}Dy_{0.1})_{9.5}Fe_{78}Co_5Nb_1B_{6.5}$ improves the coercivity from 224 kA/m to 643 kA/m after heat treatment at 710 °C for 4 min [10]. A coercivity of 575 kA/m was reported in a ribbon annealed for 20 min at 953 K, prepared from a nominal composition of $Nd_8Fe_{74}B_{14}Nb_4$ ribbons [11]. Salazar et al. reported a coercivity of 875 kA/m in $Nd_{12}Fe_{81}B_6Nb_1$ ribbons annealed at 650 °C, while a coercivity value of 405 kA/m was reported for a ribbon without Nb with a nominal composition of $Nd_{10}Fe_{84}B_6$ [12]. Nb substitution improves the magnetic properties of $Pr_8Fe_{86}B_6$ magnets, increasing the coercivity from 342 kA/m to 517 kA/m in the composition $Pr_8Fe_{86}B_6Nb_2$. Microstructural analysis revealed that Nb results in a finer and more uniform grain structure, with an average grain size between 10 and 20 nm, which enhances the magnetic performance by improving the exchange coupling between the Pr-Fe-B and α-Fe phases [13]. Furthermore, the addition of 4 at % Nb to $Nd_8Fe_{78}B_{14}$ increases coercivity from 105 kA/m to 575 kA/m after annealing at 973 K for 20 minutes. This improvement is attributed to the optimal distribution of the soft α-Fe and hard $Pr_2Fe_{14}B$ magnetic phases. Nb doping also suppresses the nucleation and growth of soft α-Fe while promoting the crystallization of hard magnetic phase [14].

The above studies are mostly based on the heat treatment of ribbons to facilitate the precipitation of soft and hard magnetic grains, enhance the exchange interaction, and improve the magnetic properties. Annealing consumes a large amount of electrical energy and time. In 2006, Chang et al. [15] reported a coercivity value of 740 kA/m for the $Pr_{8.5}Fe_{79.5}Nb_2B_{10}$ sample prepared by direct melt spinning, which is higher than that of Nb-doped ribbons with rare earth contents of 9.5 [10] and 11.5 % [9]. In addition, our recent research [16] and other reports [17, 18] have also

* Corresponding author: G. Han
E-mail: *hangb@sdu.edu.cn*

found that direct quenching can achieve higher coercivity, mainly because some amorphous phases in the sample can pin domain wall displacement or block the direct exchange between hard phase grains. Based on this, the present study investigates the influence of Nb doping and wheel speed on the magnetic performance of as-spun PrFeB nanocomposite ribbons without annealing. The objective of this study was to assess the influence of varying Nb concentrations and solidification conditions on phase formation, microstructure, and magnetic interactions between magnetic grains. By tailoring these parameters, this study aims to improve the magnetic properties, especially the coercivity (H_{cj}) of nanocomposite permanent alloys, and further clarify the primary mechanism underlying this enhancement.

2. EXPERIMENTAL DETAILS

Nominal $Pr_{10}Fe_{82.5-x}B_{6.5}Nb_x$ (x = 0, 1, 2, 3, 4) alloy ingots, each weighing 20 g, were prepared by electric arc melting under an argon atmosphere. The raw materials included high-purity (99.5 %) Pr, Fe, Nb, and FeB alloy (containing 22 wt.% B). To compensate for the evaporation loss of Pr during melting, an extra 5 wt.% was added. Each ingot was re-melted three times to ensure homogeneity, after which the oxidized surface was removed by grinding. The ingots were then broken into pieces for melt spinning into ribbons at wheel speeds of 21, 27, 30, and 33 m/s. The preparation process is shown in Fig. 1. The resulting ribbons were 0.2 – 0.3 mm thick and 4 – 5 mm long. Phase analysis of the as-spun ribbons was performed by X-ray diffraction (XRD, Smartlab-se) with Cu Kα radiation. Magnetic properties were measured using a vibrating sample magnetometer (VSM) under an applied field of 1.5 T. Microstructural analysis was carried out using a transmission electron microscope (TEM, FEI Tecnai G2 F20).

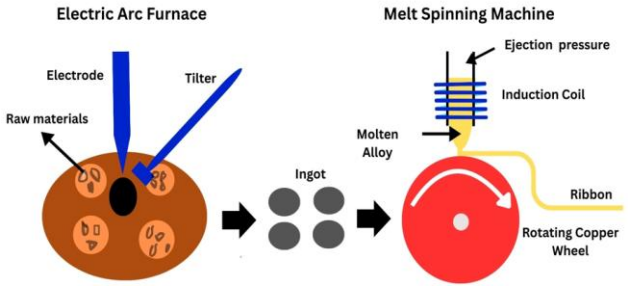

Fig. 1. Schematic diagram of the preparation process

3. RESULTS AND DISCUSSION

Fig. 2 presents the XRD patterns of melt-spun $Pr_{10}Fe_{82.5}$-$xB_{6.5}Nb_x$ (x = 0 – 4) ribbons produced at wheel speeds of 21, 27, and 33 m/s. All patterns confirm the presence of α-Fe, $Pr_2Fe_{14}B$, and an amorphous phase. The average grain size, calculated using the Scherrer equation [19], decreases with increasing wheel speed and Nb content. For the x = 0 alloy (Fig. 2 a), grain sizes are 56 nm (21 m/s), 55 nm (27 m/s), and 45 nm (33 m/s). This refining effect of wheel speed is consistent with prior reports [20]. The trend is amplified with Nb doping; for x = 1, grain sizes reduce to 52, 49, and 39 nm at the respective speeds.

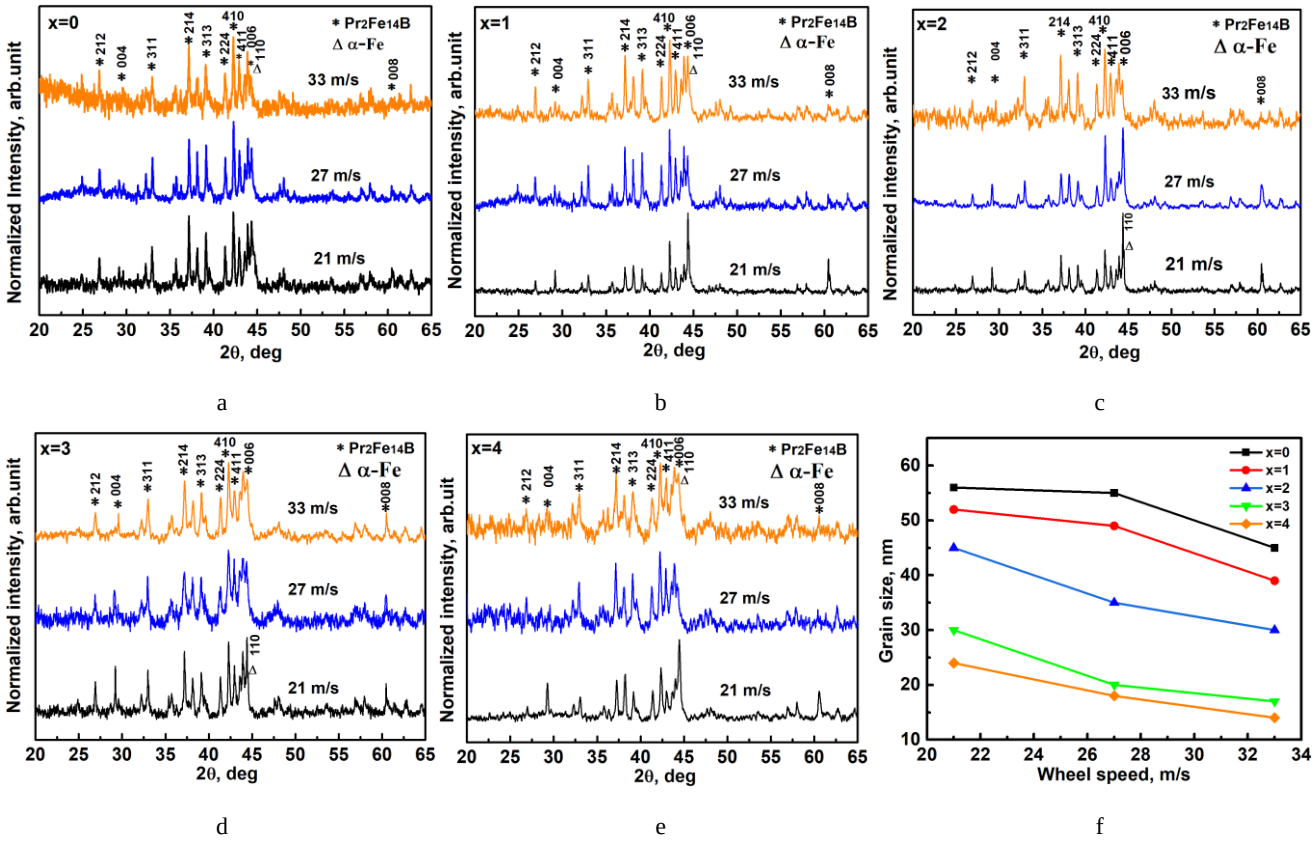

Fig. 2. Powder XRD patterns of $Pr_{10}Fe_{82.5-x}B_{6.5}Nb_x$: a – x = 0; b – x = 1; c – x = 2; d – x = 3; e – x = 4; f – grain sizes of melt-spun ribbons prepared at different wheel speeds

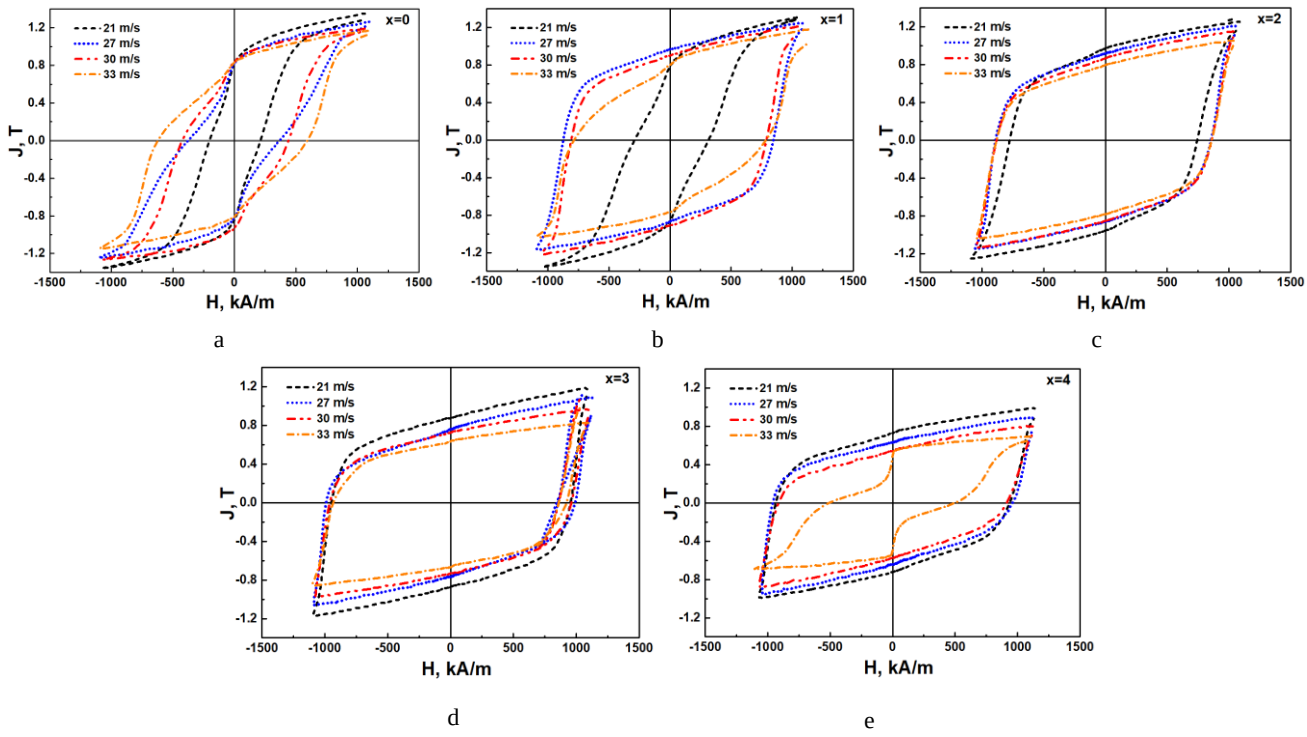

Fig. 3. Hysteresis loops of the $Pr_{10}Fe_{82.5-x}B_{6.5}Nb_x$: a – x = 0; b – x = 1; c – x = 2; d – x = 3; e – x = 4 ribbons prepared at various wheel speeds

At x = 2 (Fig. 2 c), the broader diffraction peaks correspond to further grain size refinement (45, 35, and 30 nm). This effect culminates at x = 3 and x = 4, where grain sizes are 30, 20, and 17 nm for x = 3. These results demonstrate that both an increased wheel speed and Nb doping can effectively refine the microstructure (Fig. 2 f), with Nb acting similarly to a high quenching rate in promoting amorphous phase formation.

Fig. 3 shows the hysteresis loops of $Pr_{10}Fe_{82.5-x}B_{6.5}Nb_x$ (x = 0, 1, 2, 3, 4) ribbons prepared at wheel speeds of 21 – 33 m/s. The magnetic properties were measured parallel to the ribbon plane because high values of magnetic properties were reported in the ribbon plane compared to those perpendicular to the plane [21]. To check reproducibility, we tested multiple ribbons for one composition, and found the coercivity values were very similar. For x = 0, the hysteresis loop is narrow and becomes broader at high quenching speeds. A noticeable kink appears at all wheel speeds, indicating weak exchange coupling among the magnetic grains. For x = 1, the hysteresis loop at wheel speeds of 21 and 27 m/s shows a clear visible kink, which becomes smoother and more uniform as the wheel speed increases from 30 to 33 m/s, approaching the behaviour of a single hard magnetic phase and indicating improved magnetic interaction between $Pr_2Fe_{14}B$ and α-Fe magnetic grains [22]. The interphase coupling strength can be justified from the loop squareness, which is the ratio of remanence to saturation magnetization (Jr/Js). As the wheel speed increases, the squareness of the loops (Jr/Js) for x = 1 initially increases from 0.60 (21 m/s) to 0.77 (27 m/s) and then decreases to 0.69 (33 m/s). This behaviour can be attributed to the high glass-forming ability observed at higher wheel speeds, as indicated by the XRD results shown in Fig. 2 b. For x = 2, a small kink is observed along the demagnetization curves near zero field for the ribbon prepared at a wheel speed of 21 m/s. This might be due to the incomplete intergranular exchange coupling between grains, which means that some of the large soft magnetic grains are partially or entirely disconnected from the surrounding grains and reverse independently [23]. Subsequently, with an increase in wheel speed to 27 – 33 m/s, uniform demagnetization curves are obtained. The increased squareness for x = 2 is 0.79 (27 – m/s) compared to x = 1 (0.77 at 27 m/s), likely due to the enhanced interaction between the hard and soft magnetic grains in the ribbons with x = 2. Nevertheless, with the further addition of Nb, where x = 3, the hysteresis loops at all wheel speeds exhibit increased smoothness, as illustrated in Fig. 3 d. Finally, with the addition of 4 at % Nb, the hysteresis loops at low speeds exhibit a smooth demagnetization curve, whereas a significant variation is observed at a high wheel speed of 33 ms^{-1}. This suggests that increased Nb doping and rapid quenching enhance the amorphous phase content, as evidenced by the XRD pattern shown in Fig. 2 e.

Fig. 4 a and b show the dependence of $(BH)_{max}$ and coercivity (H_{cj}) on the wheel speed for the as-spun alloys. The $(BH)_{max}$ value improves from 27 kJ/m^3 (21 m/s), to 36 kJ/m^3 (27 m/s) and 56 kJ/m^3 (33 m/s) for x = 0. With x = 1, the $(BH)_{max}$ improved from 40 kJ/m^3 (21 m/s) to 138 kJ/m^3 (27 m/s) and then reduced to 83 kJ/m^3 (33 m/s). At a wheel speed of 27 m/s, the remanence improves from 0.82 T (x = 0) to 0.96 T (x = 1), indicating that remanence enhancement occurred owing to the Nb doping. Correspondingly, the loop squareness ratio (Jr/Js) increases from 0.65 to 0.77 at 27 m/s for x = 0 and x = 1, respectively. This suggests that the highest value of 138 kJ/m^3 (for x = 1) results from the remanence enhancement, which, in turn, indicates a strong exchange coupling among the grains [23].

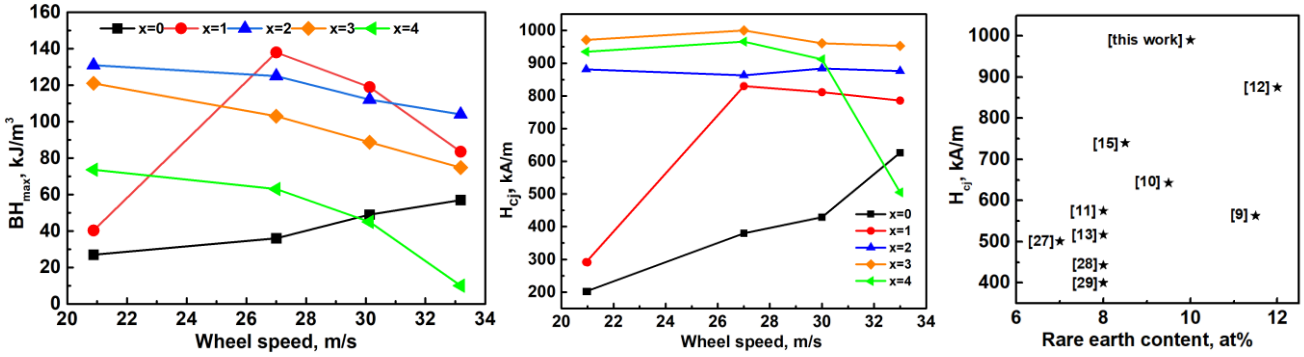

a b c

Fig. 4. a – $(BH)_{max}$; b – H_{cj} of $Pr_{10}Fe_{82.5-x}B_{6.5}Nb_x$ (x = 0, 1, 2, 3, and 4) ribbons at various wheel speeds; c – H_{cj} of nanocomposite ribbons with rare earth content of 7 – 12 at % reported so far

The $(BH)_{max}$ value decreases from 131 kJ/m^3 at 21 m/s to 92 kJ/m^3 at 30 m/s for x = 2, and from 121 kJ/m^3 at 21 m/s to 87 kJ/m^3 at 27 m/s for x = 3. Finally, for x = 4, the $(BH)_{max}$ value is 82 kJ/m^3 at 21 m/s, which then drops abruptly to 10 kJ/m^3 at 33 m/s. As the wheel speed approaches 33 m/s, the amorphous content increases, reducing the contact area between the magnetic grains. Consequently, the decoupling effect is enhanced, leading to a reduction in remanence [24]. As shown in Fig. 3 b, the large kink in the loop at 21 m/s represents weak coupling corresponding to Jr/Js = 0.60, whereas the smooth loop at 27 m/s shows strong coupling corresponding to Jr/Js = 0.77.

The coercivity (H_{cj}) of the ribbon without Nb demonstrates significant sensitivity to the wheel speed. The value increases from 202 to 626 kA/m as the wheel speed is increased from 21 to 33 m/s, as depicted in Fig. 4 b. Similarly, for x = 1, the coercivity value increases from 292 kA/m (21 m/s) to 875 kA/m (30 m/s) and thereafter decreases to 786 kA/m (33 m/s). The incorporation of x = 2 resulted in an increase in the coercivity value from 881 kA/m (21 m/s) to 883 kA/m (30 m/s), followed by a decrease to 875 kA/m (33 m/s). Moreover, the ribbon with x = 3 exhibits the highest coercivity, increasing from 971 kA/m (21 m/s) to 990 kA/m (27 m/s), before subsequently declining to 953 kA/m (33 m/s). The coercivity value of 990 kA/m is among the highest reported for nanocomposite alloys with 10 at % rare earth concentration. The incorporation of Nb markedly enhances the coercivity of the deficient rare earth nanocomposite permanent magnets [25].

The hysteresis loop for 27 m/s in Fig. 3 c displays a single hard magnetic phase characteristic, implying that the hard and soft phases are well coupled [26]. Hence, Nb content of x = 3 and wheel speed of 27 m/s are the most effective factors to attain a fine microstructure in our alloy composition. Further increasing the wheel speed decreases the coercivity value from 990 kA/m (27 m/s) to 953 kA/m (33 m/s) because of the large amorphization at higher wheel speeds [20]. Similarly, the addition of 4 % Nb decreased the coercivity, and a high (966 kA/m (27 m/s)) and low (505 kA/m (33 m/s)) values were obtained. This suggests that an excess amount of Nb doping also decreases the coercivity value due to the large amorphization, as shown by the XRD pattern in Fig. 2 e. The optimum coercivity value of 990 kA/m, remanence of 0.76 T, and $(BH)_{max}$ of 87 kJ/m^3, were achieved in the ribbon with 3 at % Nb prepared at a wheel speed of 27 m/s. A maximum $(BH)_{max}$ value of 138 kJ/m³ was achieved for x = 1 at a wheel speed of 27 m/s (Fig. 4 a). The sample shows a high remanence of 0.96 T and a large loop squareness (Jr/Js = 0.77), indicating a strong intergranular exchange coupling. With further Nb addition, the coercivity increases and reaches a maximum value of 990 kA/m for x = 3. However, this improvement in coercivity occurs at the expense of $(BH)_{max}$. The decrease in $(BH)_{max}$ is attributed to the increased amorphization and the resulting reduction in remanence, highlighting a clear trade-off between coercivity and energy product. Fig. 4 c shows the coercivity values of Nb-doped permanent nanocomposite ribbons with a rare-earth content of 7 – 12 at % reported so far. The H_{cj} value obtained in this study is even higher than that obtained with 12 at % rare earth content [12].

Fig. 5 shows the TEM and high-resolution TEM (HRTEM) images of the ribbons for x = 0 (27 m/s) and x = 3 (27 m/s). Fig. 5 a reveals a mixture of elongated and equiaxed grains with an average grain size of 37 nm. Some grains were aligned, whereas others remained randomly oriented. Fig. 5 c presents the HRTEM image of the x = 0 ribbon, which further clearly shows that the 2:14:1 phase is the main phase. As shown in Fig. 5 b, the addition of 3 at % Nb reduces the grain size, resulting in an average grain size of approximately 26 nm, which enhances the exchange interactions among the grains [16], leading to a significant increase in coercivity from 380 kA/m (x = 0) to 990 kA/m (x = 3). Fig. 5 d shows a high-resolution TEM image of the alloy with 3 at % Nb, which reveals a clear and continuous (002) lattice plane with an interplanar spacing of around 0.640 nm, indicating a strong long-range crystallographic order. In contrast, the (006), (004), and (214) planes appear to be more randomly oriented, indicating short-range ordering. In addition, the existence of fine amorphous regions within the matrix may contribute to domain wall pinning, which is essential for enhanced coercivity. To investigate the influence of microstructure on intergranular exchange interactions, we checked the recoil loops of the ribbons. In this regard, the recoil permeability values μ_{rec} are slopes deduced from the recoil loops.

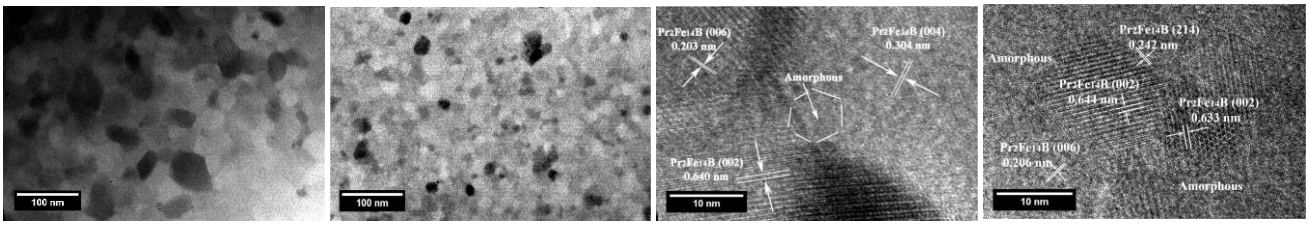

a b c d

Fig. 5. a, c – TEM and HRTEM images of $Pr_{10}Fe_{82.5}B_{6.5}$; b, d – of $Pr_{10}Fe_{79.5}B_{6.5}Nb_3$ ribbons prepared at a wheel speed of 27 m/s

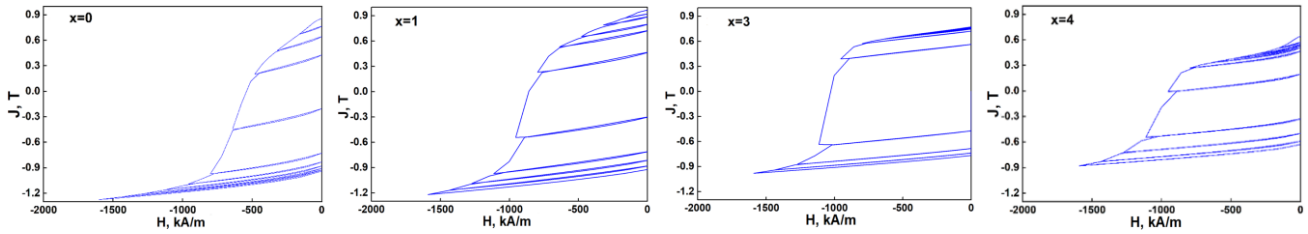

a b c d

Fig. 6. Recoil loops for $Pr_{10}Fe_{82.5-x}B_{6.5}Nb_x$: a – x = 0; b – x = 1; c – x = 3; d – x = 4 melt-spun ribbons prepared at the wheel speed of 27 m/s

Fig. 6 demonstrates the recoil loops for $Pr_{10}Fe_{82.5-x}B_{6.5}Nb_x$ (x = 0, 1, 3, and 4) melt-spun ribbons prepared at the wheel speed of 27 m/s. For x = 0, the recoil permeability μ_{rec} ranges from 31.0 to 1.133 (10^{-4} T)/(kA/m) from low to high external field. For x = 1, the permeability μ_{rec} decreases to 5.66 ($\times 10^{-4}$ T)/(kA/m) (low field) and 1.83 (10^{-4} T)/(kA/m) (high field). With the addition of x = 3, the material exhibits single-phase magnetic characteristics with permeability μ_{rec} value from 2.53 to 1.32 (10^{-4} T)/(kA/m) from low to high field. The lowest permeability value suggests a strong exchange coupling between the grains, leading to the concurrent reversal of soft and hard phases [30], which means the strong exchange coupling interaction between soft and hard magnetic grains can constrain the magnetic behaviour, and makes the two phases switch their magnetic orientations simultaneously under an external magnetic field.

Furthermore, the small opening of the recoil loops at low external fields indicates minimal permeability, consistent with single hard magnetic phase behaviour. This is supported by the corresponding XRD pattern for the 3 at % Nb sample (Fig. 2 d), where the high-intensity peaks predominantly belong to the 2:14:1 phase. In contrast, the recoil loops for x = 4 exhibit a two-phase magnetic characteristic, with the permeability μ_{rec} increasing from 8.91 to 1.72 (10^{-4} T)/(kA/m). However, a single-phase magnetic character is observed at higher fields approaching the coercive field. This suggests that the soft magnetic phase reverses at low applied fields before that of the hard magnetic grains, indicating the coexistence and independent reversal of both phases at low fields. Compared to that with x = 3, the sample with x = 4 shows an increased permeability range and a greater loop openness (Fig. 6 d), indicating relatively weak exchange coupling and consequently lower coercivity, as confirmed by the hysteresis loops in Fig. 3 e.

To investigate the magnetization process, Fig. 7 presents the initial magnetization curves for $Pr_{10}Fe_{82.5-x}B_{6.5}Nb_x$ (x = 0, 1, 3, 4) ribbons prepared at wheel speeds of 21 – 33 m/s. For x = 0, the initial magnetization curves suggest that the coercivity mechanism is primarily governed by the nucleation of reversed domains for ribbons spun at 21, 27, and 30 m/s. A slight curvature at 33 m/s hints at the onset of a domain wall pinning mechanism. For x = 1, the initial curve at 21 m/s indicates a nucleation mechanism, while the curves become progressively steeper from 27 to 33 m/s, suggesting strengthening domain wall pinning with increasing wheel speed. At 33 m/s, the initial curve reveals a mixed coercivity mechanism: initial nucleation followed by domain wall pinning. With both the Nb content and wheel speed increasing, the domain wall pinning strength is enhanced, as shown in Fig. 7 b. Similarly, for x = 3, a steeper initial magnetization curve is observed, correlating with a high coercivity of 990 kA/m at 27 m/s. XRD patterns (Fig. 2 a – d) indicate that the amorphous content increases with both the increasing quenching speed and Nb content.

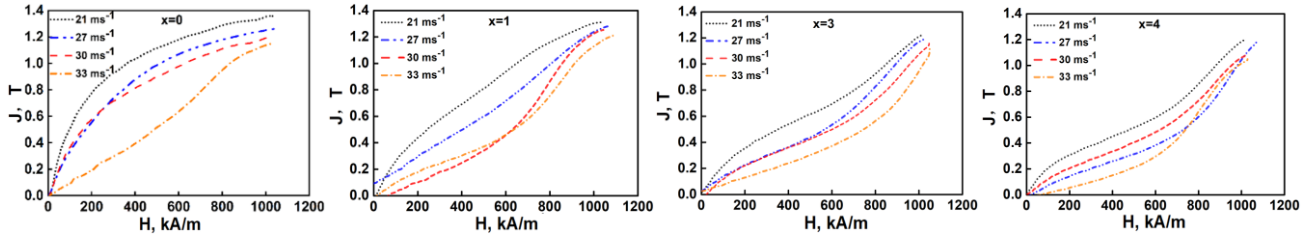

a b c d

Fig. 7. Initial magnetization curves for ribbons: a – x = 0; b – x = 1; c – x = 3; d – x = 4 prepared at wheel speeds of 21 to 33 m/s

This leads to the formation of intergranular amorphous layers between nanocrystals, which pins domain wall motion and thereby increases the coercivity [31 – 33]. The initial magnetization curves clearly demonstrate that Nb doping enhances the pinning strength and corresponding coercivity. For $x = 4$, the initial magnetization curve is also steep, and the coercivity value is just a little below that of $x = 3$. A substantial amorphous phase revealed by the XRD pattern (Fig. 2 e) may degrades the magnetic properties and overall performance compared to that with $x = 3$.

4. CONCLUSIONS

$Pr_{10}Fe_{82.5-x}B_{6.5}Nb_x$ ribbons with varying Nb concentrations ($x = 0, 1, 2, 3, 4$) were synthesized by using the electric arc furnace and melt spinning machine. XRD and TEM results indicate that Nb doping significantly refines the grain size and enhances coercivity. The coercivity (H_{cj}) improves from 380 ($x = 0$) to 990 kA/m ($x = 3$), which is among the highest values reported for rare-earth-deficient nanocomposite alloys with Nb doping. This improvement can be attributed to the refined microstructure and reduced grain size resulting from Nb addition. Recoil loop analysis reveals that Nb doping strengthens the exchange coupling. The sample with $x = 3$ exhibits the smallest recoil permeability values of 2.53×10^{-4} T/(kA/m) at low field and 1.32×10^{-4} T/(kA/m) at high field, indicating the strong exchange coupling between the hard and soft magnetic phases. The initial magnetization curves (IMC) further confirm a transition from domain nucleation to domain wall pinning mechanisms with increasing Nb content. The $x = 3$ composition exhibits dominant domain wall pinning, leading to the highest coercivity. This study demonstrates that Nb doping is an effective approach for optimizing both the microstructure and magnetic properties in low-rare-earth systems, offering a cost-effective magnet solution for advanced magnetic applications. These findings provide a practical route for developing high-performing and sustainable rare-earth magnets, by reducing the amount of critical rare-earth elements and energy required for annealing.

Acknowledgments

This research received financial support from the National Natural Science Foundation of China (12074220, 52171158). We thank Kuai from Core Facility Sharing Platform of Shandong University for XRD support.

REFERENCES

1. **Zhu, X.D., Wang, M., Yu, Y.J., Wang, Q., Wang, F., Wang, P.F., Jia, B., Wang, C., Zhou, B.** Coercivity Enhancement of Sintered Nd-Pr-Fe-B Magnets by Cost-effective Grain Boundary Diffusion of Dy/Tb Films *Crystals* 13 (10) 2023: pp. 1516 https://doi.org/10.3390/cryst13101516
2. **Mican, S., Hirian, R., Isnard, O., Chicinas, I., Pop, V.** Effect of Milling Conditions on the Microstructure and Interphase Exchange Coupling of $Nd_2Fe_{14}B$/α-Fe Nanocomposites *Physics Procedia* 75 2015: pp. 1314. https://doi.org/10.1016/j.phpro.2015.12.147
3. **Ding, H.W., Cui, C.X., Yang, W., Sun, J.B.** Effects of Cobalt Addition on Microstructure and Magnetic Properties of PrNdFeB/Fe_7Co_3 Nanocomposite *Journal of Rare Earths* 35 (5) 2017: pp. 468 – 473. https://doi.org/10.1016/S1002-0721(17)60935-9
4. **Chen, P., Kou, J.Y., Lou, L., Hua, Y.X., Li, T.C., Gao, J.Q., Wan, Y., Yang, L.Q., Guo, D.F., Li, X.H., Li, W.** Suppression of Metastable Phases in $Nd_2Fe_{14}B$/α-Fe Nanocomposite Magnets Through Laser-heated Annealing with Ultrafast Heating Rates *Physica Scripta* 100 (5) 2025: pp. 055915. https://doi.org/10.1088/1402-4896/adc2ad
5. **Kou, J.Y., Zheng, Y., Lou, L., Hua, Y.X., Chen, P., Bi, Z.W., Song, P., Li, X.H., Guo, D.F.** Bulk Anisotropic $Nd_2Fe_{14}B$/α-Fe Nanocomposite Magnet Prepared by Hot Rolling *Journal of Magnetism and Magnetic Materials* 591 2024: pp. 171733. https://doi.org/10.1016/j.jmmm.2024.171733
6. **Wang, L., Quan, Q.C., Zhang, L.L., Hu, X.J., Rehman, S.U., Jiang, Q.Z., Du, J.F., Zhong, Z.C.** Microstructures, Magnetic Properties and Coercivity Mechanisms of Nd-Ce-Fe-B Based Alloys by Zr Substitution *Journal of Applied Physics* 123 (11) 2018: pp. 113904. https://doi.org/10.1063/1.5018461
7. **Goll, D., Kronmüller, H.** High-performance Permanent Magnets *Naturwissenschaften* 87 (10) 2000: p. 423 – 438. https://doi.org/10.1007/s001140050755
8. **Zhang, W.Y., Kharel, P., Al-Omari, I.A., Shield, J.E., Sellmyer, D.J.** Effect of Element Substitution on Nanostructure and Hard Magnetism of Rapidly Quenched $Nd_2Fe_{14}B$ *Philosophical Magazine* 96 (26) 2016: pp. 2800 – 2807. https://doi.org/10.1080/14786435.2016.1215608
9. **Jun, L., Ying, L., Ma, Y.L.** Effect of Niobium on Microstructure and Magnetic Properties of Bulk Anisotropic NdFeB/α-Fe Nanocomposites *Journal of Magnetism and Magnetic Materials* 324 (14) 2012.: pp. 2292 – 2297. https://doi.org/10.1016/j.jmmm.2012.02.118
10. **Wang, Z.Y., Liu, W.Q., Zhou, B.X., Ni, J.S., Xu, H., Li, Q.** Microstructural Characteristics of $Nd_2Fe_{14}B$/α-Fe Nanocomposite Ribbons Bearing Nb Element *Rare Metals* 27 (3) 2008: pp. 299 – 302. https://doi.org/10.1016/S1001-0521(08)60133-3
11. **Derewnicka-Krawczynska, D., Ferrari, S., Bilovol, V., Pagnola, M., Morawiec, K., Saccone, F.D.** Influence of Nb, Mo, and Ti as Doping Metals on Structure and Magnetic Response in NdFeB Based Melt Spun Ribbons *Journal of Magnetism and Magnetic Materials* 462 2018: pp. 83 – 95. https://doi.org/10.1016/j.jmmm.2018.05.004
12. **Salazar, D., Martín-Cid, A., Madugundo, R., Garitaonandia, J.S., Barandiaran, J.M., Hadjipanayis, G.C.** Effect of Nb and Cu on the Crystallization Behavior of Under-stoichiometric Nd–Fe–B Alloys *Journal of Physics D: Applied Physics* 50 (1) 2016: pp. 015305. https://doi.org/10.1088/1361-6463/50/1/015305
13. **Chen, Z.M., Okumura, H., Hadjipanayis, G.C., Chen, Q.** Microstructure Refinement and Magnetic Property Enhancement of Nanocomposite $Pr_2Fe_{14}B$/α-Fe Magnets by Small Substitution of M for Fe (M= Cr, Nb, Ti and Zr) *Journal of Alloys and Compounds* 327 (1 – 2) 2001: pp. 201 – 205. https://doi.org/10.1016/S0925-8388(01)01418-9
14. **Bilovol, V., Ferrari, S., Pampillo, L.G., Derewnicka, D., Spyra, M., Saccone, F.D.** Influence of Nb Doping on Magnetic Properties of Nanocrystalline Nd-Fe-B Alloys

IEEE Transactions on Magnetics 49 (8) 2013: pp. 4622 – 4625. https://doi.org/10.1109/TMAG.2013.2257707

15. **Chang, H.W., Chiu, C.H., Chang, C.W., Chen, C.H., Chang, W.C., Sun, A.C., Yao, Y.D.** Comparison on the Phase Evolution and Magnetic Properties of Direct-quenched $Pr_{8.5}Fe_{79.5}M_2B_{10}$ (M= Cr, Nb, Ti, V, and Zr) Ribbons *Journal of Magnetism and Magnetic Materials* 304 (1) 2006: pp. e216 – e218. https://doi.org/10.1016/j.jmmm.2006.01.200
16. **Alam, M.K., Han, G., Kang, S.** Effect of P and Zr on the Microstructure and Magnetic Properties of Nanocomposite $Pr_2Fe_{14}B$/α-Fe Ribbons *Journal of Magnetism and Magnetic Materials* 517 2021: pp. 167345. https://doi.org/10.1016/j.jmmm.2020.167345
17. **Singh, S., Diraviam, A.B., Sarkar, R., Haldar, A., Muthuvel, M.** Effect of Quenching Rate on the Structural and Hard Magnetic Properties of Nd-Fe-B Melt-spun Ribbons *AIP Advances* 13 2023: pp. 025301. https://doi.org/10.1063/9.0000524
18. **Nguyen, X.T., Nguyen, V.V.** Preparation and Magnetic Properties of Bi-doped NdFeB-Based Melt-spun Nanocrystalline Ribbons *Advances in Natural Sciences: Nanoscience and Nanotechnology*. 16 2025: pp. 045004. https://doi.org/10.1088/2043-6262/adf96f
19. P**atterson, A.L.** The Scherrer Formula for X-Ray Particle Size Determination *Physical Review* 56 (10) 1939: pp. 978 – 982. https://doi.org/10.1103/PhysRev.56.978
20. **Mendoza-Suárez, G., Escalante-García, J.I., López-Cuevas, J., Vargas-Gutiérrez, G., Mancha-Molinar, H., Mendez-Nonell, J.** Effect of Roll Speed on the Magnetic Properties of Nanocomposite PrFeB Magnets Prepared by Melt-spinning *Journal of Magnetism and Magnetic Materials* 206 (1 – 2) 1999: pp. 37 – 44. https://doi.org/10.1016/S0304-8853(99)00516-8
21. **Zhang, X.Y., Guan, Y., Yang, L., Zhang, J.W.** Crystallographic Texture and Magnetic Anisotropy of α-Fe/$Nd_2Fe_{14}B$ Nanocomposites Prepared by Controlled Melt Spinning *Applied Physics Letters* 79 (15) 2001: pp. 2426 – 2428. https://doi.org/10.1063/1.1409269
22. **Pan, M.X., Li, Z., Wu, Q., Ge, H.L., Xu, H.** Study of the Role of Ti Doping on Magnetic Properties of some Nanocomposite Alloys of α-Fe/$Nd_2Fe_{14}B$ Type *Journal of Magnetism and Magnetic Materials* 471 2019: pp. 457 – 463. https://doi.org/10.1016/j.jmmm.2018.09.097
23. **Wang, Z.C., Zhou, S.Z., Zhang, M.C., Qiao, Y., Wang, R.** Effects of As-quenched Structures on the Phase Transformations and Magnetic Properties of Melt-spun $Pr_7Fe_{88}B_5$ Ribbons *Journal of Applied Physics* 86 (12) 1999: pp. 7010 – 7016. https://doi.org/10.1063/1.371787
24. **Wang, L., Wang, J., Rong, M.H., Rao, G.H., Zhou, H.Y.** Effect of Wheel Speed on Phase Formation and Magnetic Properties of ($Nd_{0.4}La_{0.6}$)-Fe-B Melt-spun Ribbons *Journal of Rare Earths* 36 (11) 2018: pp. 1179 – 1183. https://doi.org/10.1016/j.jre.2018.02.013
25. **Spyra, M., Derewnicka, D., Leonowicz, M.** Lean Neodymium Nd–Fe–B Magnets Containing Minor Addition of Titanium *Physica Status Solidi (A)* 207 (5) 2010: pp. 1170 – 1173. https://doi.org/10.1002/pssa.200983395
26. **Yang, S., Liu, X.S., Li, S.D., Xie, G.Z., Song, X.P., Gu, B.X., Du, Y.W.** Effect of Wheel Speed on the Microstructure and Exchange Coupling Interaction of Nanocomposite $Nd_2Fe_{14}B$/α-Fe Magnets *Materials Science and Engineering: A* 347 (1 – 2) 2003: pp. 325 – 329. https://doi.org/10.1016/S0921-5093(02)00606-8
27. **Chiu, C.H., Chang, H.W., Chang, W.C.** Effect of Fe Substitution by Ti or Nb/V/Zr on Phase Stability and Magnetic Properties of $Pr_2Fe_{23}(B, C)_3$ Ribbons *Journal of Magnetism and Magnetic Materials* 282 2004: pp. 186 – 192. https://doi.org/10.1016/j.jmmm.2004.04.043
28. **Yang, C.J., Han, J.S., Park, E.B., Kim, EC.** Characterization of Intergranular Phase in $Nd_8Fe_{86-x}Nb_xB_6$ (x= 0, 1, 2, 3) Nanocomposite Magnet by Mössbauer Spectroscopy *Journal of Magnetism and Magnetic Materials* 301 (1) 2006: pp. 220 – 230. https://doi.org/10.1016/j.jmmm.2005.06.031
29. **Betancourt, I., Davies, H.** Influence of Zr and Nb Dopant Additions on the Microstructure and Magnetic Properties of Nanocomposite $RE_2(Fe, Co)_{14}B$/α-(Fe, Co)(RE= Nd–Pr) Alloys *Journal of Magnetism and Magnetic Materials* 261 (3) 2003: pp. 328 – 336. https://doi.org/10.1016/S0304-853(02)00366-9
30. **Alam, M.K., Han, G.B., Kang, S.S.** High Coercivity $Pr_2Fe_{14}B$/α-Fe Nanocomposite Permanent Magnets with Zr Addition *Rare Metals* 39 (1) 2020: pp. 41 – 47. https://doi.org/10.1007/s12598-019-01258-7
31. **Alam, M.K., Raza, S., Gao, C.Y., Han, G.B., Kang, S.S.** Cu-doped Nanocomposite $Pr_2Fe_{14}B$/α-Fe Ribbons with High $(BH)_{max}$ *Chinese Physics B* 33 (12) 2024: pp. 127504. https://doi.org/10.1088/1674-1056/ad8cba
32. **Zhang, Y.M., Li, W., Li, H.L., Zhang, X.Y.** Coercivity Mechanism of α-Fe/$Nd_2Fe_{14}B$ Nanocomposite Magnets with an Intergranular Amorphous Phase *Journal of Physics D: Applied Physics* 47 (1) 2013: pp. 015002. https://doi.org/10.1088/0022-3727/47/1/015002
33. **Chen, F.G., Zhang, T.Q., Wang, J., Zhang, L.T., Zhou, G.F.** Investigation of Domain Wall Pinning Effect Induced by Annealing Stress in Sintered Nd–Fe–B Magnet *Journal of Alloys and Compounds* 640 2015: pp. 371 – 375. https://doi.org/10.1016/j.jallcom.2015.04.017